Journal of Applied Physics ARTICLE scitation.org/journal/jap

A simulation-based study on water radiolysis species for $^{1}H^{+}$, $^{4}He^{2+}$, and $^{12}C^{6+}$ ion beams with multiple ionization using Geant4-DNA

Cite as: J. Appl. Phys. **129**, 244702 (2021); doi: 10.1063/5.0054665
Submitted: 20 April 2021 · Accepted: 10 June 2021 ·
Published Online: 30 June 2021

Kentaro Baba,[1] Tamon Kusumoto,[2] Shogo Okada,[3] and Masayori Ishikawa[1,4,a)]

AFFILIATIONS

[1]Graduate School of Biomedical Science and Engineering, Hokkaido University, Kita-15 Nishi-7, Kita-ku, Sapporo, Hokkaido 060-8638, Japan
[2]National Institutes for Quantum and Radiological Science and Technology, 4-9-1 Anagawa, Inage-ku, Chiba 263-8555, Japan
[3]High Energy Accelerator Research Organization (KEK), 1-1, Oho, Tsukuba, Ibaraki 305-0801, Japan
[4]Faculty of Health Sciences, Hokkaido University, Kita-12 Nishi-5, Kita-ku, Sapporo, Hokkaido 060-0812, Japan

[a)]**Author to whom correspondence should be addressed:** masayori@med.hokudai.ac.jp

ABSTRACT

Monte Carlo track structure simulation is a powerful method for estimating damage induced by water radiolysis products for cell killing. To investigate the influence of multiple ionization for the formation of water radiolysis products under $^{1}H^{+}$, $^{4}He^{2+}$, and $^{12}C^{6+}$ ion beams, a Monte Carlo simulation based on Geant4-DNA was carried out. The G-value of H_2O_2 increased monotonically with increasing linear energy transfer up to 200 eV/nm. Above 200 eV/nm, the G-value of H_2O_2 began dropping, but only when the influence of multiple ionization was considered. This trend is in good agreement with the experimental results. Furthermore, we successfully reproduce the experimental results of G-values of $HO_2^{\bullet} + O_2^{\bullet-}$. The role of the multiple ionization in the production of H_2O_2, $HO_2^{\bullet}$, $O_2^{\bullet-}$, and O_2 is also discussed.

INTRODUCTION

Radiation therapy by external beam irradiation is an established treatment option for solid cancer tumors. Heavy-ion therapy is especially effective for deep-seated tumors and hypoxic tumors,[1,2] compared to proton and conventional x-ray therapies, resulting in high relative biological effectiveness (RBE). Oxygen enhancement ratio (OER) is also an important factor for estimating the effectiveness of radiation therapy. RBE and OER strongly depend on linear energy transfer (LET). Higher values of RBE correspond with high effectiveness, whereas lower values of OER ($\geq$1) indicate less influence of oxygen concentration. In the case of the $^{12}C^{6+}$ ion beam, the value of RBE is maximum at a LET of 140 keV/μm (=eV/nm), then drops.[3] The value of OER of the $^{12}C^{6+}$ ion beam is about 3 in the low-LET region. The value of OER decreases monotonically with increasing LET and reaches about 1 above 200 eV/nm. In practical terms, the effectiveness of $^{12}C^{6+}$ ion beam therapy for hypoxic tumors is higher than that of x-ray because of its high LET. However, the influence of oxygen concentration of tumors on cell killing ability by heavy ions is not negligible.[4,5] It has also been suggested that changes in oxygen concentration in tumors are important to elucidate the mechanism of a newly developed cancer therapy performed under ultrahigh dose rates (>40 Gy/s), called FLASH therapy. The effect of oxygen concentration in tumors should be accurately considered for reliable treatment.[6–8]

It is well known that cell killing due to DNA damage is suppressed under hypoxia conditions; however, the mechanism of OER is still unclear. Even hypoxic tumors are killed in the high-LET region, meaning that the value of OER approaches 1. A plausible interpretation of this mechanism is the influence of "oxygen-in-the-track," in which the interaction between water radiolysis products generates oxygen molecules. Water radiolysis products are generated in a certain region, generally known as a "spur," which might be spherical. Spurs become continuous with increasing LET, consequently forming a cylindrical shape in high-LET regions. Because the value of OER decreases with increasing LET,

above 200 eV/nm, in which a continuous spur can be expected, oxygen molecules are supplied due to reactions between water radiolysis products. It has been noted that the influence of oxygen depletion of hypoxic tumors could be minimized.[9] Namely, we should investigate the role played by reactions between water radiolysis products to explain why the value of OER reduces with increasing LET.

Many researchers have made efforts to clarify the mechanism of reactions between water radiolysis products through experiments and computer simulations. One of the results suggested that multiple ionization plays an important role in generating $O_2^{\bullet-}$ and $HO_2^{\bullet}$.[10] Additionally, multiple ionization has to be considered to accurately estimate yields of H_2O_2.[10–12] Indeed, we previously validated the experimental results of the yields of •OH and e_{aq}^- in a wide LET region, including the Bragg peak energy of $^4He^{2+}$ and $^{12}C^{6+}$ ion beams, using a Monte Carlo simulation based on Geant4-DNA. However, the yield of H_2O_2 had discrepancies between simulation and experimental results.[13] We hypothesized that the discrepancies could be due to the lack of multiple ionization processes. In this study, we aim to understand the contribution of multiple ionization under $^1H^+$, $^4He^{2+}$, and $^{12}C^{6+}$ ion beams, whose roles are not taken into account in the latest version of Geant4 ver. 10.07.p01. We added physics, physicochemical, and chemical processes and validated the simulation results by comparing them with experimental results. The simulation-based evaluation was carried out for the radiation chemical yields (G-value) of $O_2^{\bullet-}$, $HO_2^{\bullet}$, and H_2O_2 under $^1H^+$, $^4He^{2+}$, and $^{12}C^{6+}$ ion beams with LET range from 2 to 700 eV/nm. One of the biggest motivations in this study is the development of Geant4. We hope to contribute to this radiation simulator, which covers from physical stage to biological stage and is freely available to everyone in the world.

MATERIALS AND METHODS

Geant4[14–16] is a simulation toolkit written in C++ language for simulations of passages of particles through matter with the Monte Carlo method. Geant4 has an extension package named Geant4-DNA[17–20] for track structures of charged particles and radiochemical reactions at subcellular scales. We used Geant4-DNA delivered by Geant4 version 10.07.p01 to obtain G-values of water radiolysis products through chemistry simulations with the step-by-step approach.[21,22] The definition of G-value is the number of species formed or destroyed per unit energy (traditionally 100 eV) absorbed by media. In this work, we follow the radical annihilation process from 1 ps to 1 μs under neutral pH conditions at 25 °C.

For the physics stage, we used the *G4EmDNAPhysics_option8* physics list implemented in Geant4-DNA. Similar trends can be seen with other physics options, but *G4EmDNAPhysics_option8* reproduced experimental results the best. Elastic scattering, ionization, and electronic excitation processes for electrons, protons, neutral hydrogen atoms, and helium atoms with three charged states ($^4He^0$, $^4He^+$, and $^4He^{++}$) were taken into account. Sub-excitation processes of vibrational excitation and molecular attachment for electrons and charge exchange process for protons, neutral hydrogen atoms, and charged helium atoms were considered. For heavy ions ($^7Li^{3+}$, $^9Be^{4+}$, $^{11}B^{5+}$, $^{12}C^{6+}$, $^{14}N^{7+}$, $^{16}O^{8+}$, $^{28}Si^{14+}$, and $^{56}Fe^{26+}$), we considered an ionization process with effective charge scaling.[17–20] We obtained the distribution of energy loss of charged particles in water medium through the physics stage of Geant4-DNA simulations. When primary particles have deposited 10 keV of their energies into the water, the charged particle tracking simulation of the physical process was ceased and shifted to the chemical process. We aborted the event when total energy deposition of each event exceeded 10.1 keV in order to simulate large enough numbers of tracks in reasonable calculation times. That means that total energy deposition of each event was always between 10 and 10.1 keV. In the present study, an air-free water volume of $10 \times 10 \times 10$ mm^3 was set as the target.

Geant4-DNA ver. 10.07.p01 does not provide a multiple ionization process under proton ($^1H^+$) and heavy ions ($^4He^{2+}$ and $^{12}C^{6+}$). It is also not implemented in Geant4 ver. 10.07.p01. We challenged to implement multiple ionization as additional physics, physicochemical, and chemical processes of Geant4-DNA, including calculations of cross sections for double and triple ionization of water. It is based on the *G4DNARuddIonisationExtendedModel* class. The cross section values of double ionization (σ_{di}) were deduced from Rudd's single ionization cross sections (σ_{si}) for water vapor.[23,24] Unfortunately, the available information on the cross sections for the double and triple ionization of water is still quite limited.[11,25] We used the ratio ($\alpha = \sigma_{di}/\sigma_{si}$) from the data sets proposed by Meesungnoen and Jay-Gerin.[11] Details are mentioned in their previous studies.[10,11,26,27] It is an adjustable parameter to reproduce the measured G-value of $HO_2^{\bullet} + O_2^{\bullet-}$ strongly affected by multiple ionization. The cross section values of triple ionization (σ_{ti}) are about one order of magnitude lower than σ_{di}.[25] We therefore ignored the influence of quadruple ionization as it adds only a minor contribution to the G-value of H_2O_2, $HO_2^{\bullet}$, and $O_2^{\bullet-}$.[10,11] In the range of LET considered in this work, σ_{ti} was set as $\sigma_{ti} = \alpha^2\sigma_{si}$.[11] Tables I and II show the decomposition reaction schemes and parameters in the physicochemical process.[12]

At the physicochemical stage, water molecules are excited or ionized, resulting in the production of other molecular species such as radicals, ions, and molecules. For the chemical stage, the *G4EmDNAChemistry* constructor with additional reactions was used. The list of reactions and reaction rate constants is shown in Table III. The reactions in Table III are taken from Ref. 13 and modified with the addition of reactions (R1), (R2), and (R3). The reaction rate constants were referred from previous studies.[28,29] $HO_2^{\bullet}$ and $O_2^{\bullet-}$ are mainly produced from multiple ionization of water through oxygen atoms formed in their ^3P ground state.[11] The ground-state O(^3P) atoms will react with themselves or with

TABLE I. The branching ratio of dissociation channels used for simulation of the physicochemical stage in liquid water.[30]

Single ionization state: H_2O^+	→	$H_3O^+ + \bullet OH$	100%
Excitation state: A1B1	→	$\bullet OH + H^{\bullet}$	65%
	→	$H_2O + \Delta E$	35%
Excitation state: B1A1	→	$H_3O^+ + \bullet OH + e_{aq}^-$	55%
	→	$\bullet OH + \bullet OH + H_2$	15%
	→	$H_2O + \Delta E$	30%
Excitation state:	→	$H_3O^+ + \bullet OH + e_{aq}^-$	50%
Rydberg, diffusion bands	→	$H_2O + \Delta E$	50%
Dissociate attachment	→	$\bullet OH + OH^- + H_2$	100%

TABLE II. Dissociation channels related to multiple ionization events at the physicochemical stage. The distances between the fragments are given in nanometers.[12]

Double ionization state: H_2O^{2+}	→	$H^+ + H^+ + O(^3P)$	→	$2H_3O^+ + O(^3P)$	55%	$d_{O-H^+} = 1.20$
	→	$H^+ + OH^+$	→	$2H_3O^+ + O(^3P)$	29%	$d_{H^+-OH^+} = 1.20$
	→	$H^+ + H^\bullet + O^+$	→	$2H_3O^+ + H^\bullet + \bullet OH + O(^3P)$	16%	$d_{H^+-O^+} = 1.20$
						$d_{H_\bullet-O^+} = 0.80$
Triple ionization state: H_2O^{3+}	→	$H^+ + H^+ + O^+$	→	$3H_3O^+ + \bullet OH + O(^3P)$	100%	$d_{O^+-H^+} = 1.20$

•OH in the track core of the impacting ions because of the very high local concentration of radicals.[11,27] The following reactions (R1), (R2), and (R3) have been added to consider the above estimation. These reaction rate constants are based on the data of Hatano *et al.*,[28]

$$\bullet OH + O(^3P) \rightarrow HO_2^\bullet \quad 2.02 \times 10^{10}\ (dm^3\ mol^{-1}\ s^{-1}), \qquad (R1)$$

$$O(^3P) + O(^3P) \rightarrow O_2 \quad 2.2 \times 10^{10}\ (dm^3\ mol^{-1}\ s^{-1}), \qquad (R2)$$

$$HO_2^\bullet + O(^3P) \rightarrow O_2 + \bullet OH \quad 2.02 \times 10^{10}\ (dm^3\ mol^{-1}\ s^{-1}). \qquad (R3)$$

RESULTS AND DISCUSSION

The ratio of double-to-single ionization cross sections $\alpha = \sigma_{di}/\sigma_{si}$ is referred to as Meesungnoen's value (Fig. 1).[11] The value of σ_{di}/σ_{si} decreases monotonically with increasing E_{ion}/Z, where E_{ion} is the ion energy per nucleon and Z is the projectile charge state. This means that the influence of double ionization increases monotonically with increasing LET. Using these values of σ_{di}/σ_{si} in our simulation of the radiolysis of pure neutral water with $^1H^+$, $^4He^{2+}$, and $^{12}C^{6+}$ ion beams, we then calculated the G-values of H_2O_2 and $HO_2^\bullet + O_2^{\bullet-}$ as a function of LET.

Figure 2 shows the LET dependence of the G-values of H_2O_2 at 1 μs after irradiation. The simulated G-values and experimental results are shown in colored and black symbols, respectively[31–36] Solid and dotted lines represent the trends obtained by Genat4-DNA simulation with and without the multiple ionization processes, respectively. In the case of experiments around Bragg peak energies, incoming ions completely stop in the irradiation cell. Thus, energies of incoming ions (i.e., LET) vary drastically. Around the Bragg peak region, the number of water radiolysis species N is estimated by the integration over the ion trajectory. Generally, N increases monotonically with the energy of incident ions E_0.[37] The G-value can be evaluated from the differential value at certain energies. Significant differences of G-values of H_2O_2 for the $^1H^+$ ion beam are not observed, whether or not multiple ionization is taken into account. The simulated G-value for the $^1H^+$ ion beam is in better agreement with experimental data obtained by Wasselin-Trupin *et al.*,[36] rather than Pastina and LaVerne,[34] Burns and Sims,[33] and Anderson and Hart.[31] A similar trend is seen in the G-value of H_2O_2 for $^4He^{2+}$ ion beams. The increasing behavior of G-value is slowing down above 50 eV/nm, when we consider the role of the multiple ionization. The simulated G-values for the

TABLE III. Reaction and reaction rate constants. These values are based on the data of Hatano *et al.*[28] and Plante.[29]

Reaction	Reaction rate ($dm^3\ mol^{-1}\ s^{-1}$)	Reaction	Reaction rate ($dm^3\ mol^{-1}\ s^{-1}$)
$H^\bullet + H^\bullet \rightarrow H_2$	5.03×10^9	$H_2O_2 + e_{aq}^- \rightarrow OH^- + \bullet OH$	1.1×10^{10}
$H^\bullet + {}^\bullet OH \rightarrow$ No product	1.55×10^{10}	$H_2O_2 + OH^- \rightarrow HO_2^-$	4.75×10^8
$H^\bullet + H_2O_2 \rightarrow \bullet OH$	3.5×10^7	$H_2O_2 + O^{\bullet-} \rightarrow HO_2^\bullet + OH^-$	5.55×10^8
$H^\bullet + e_{aq}^- \rightarrow H_2 + OH^-$	2.5×10^{10}	$e_{aq}^- + e_{aq}^- \rightarrow 2OH^- + H_2$	5.0×10^9
$H^\bullet + OH^- \rightarrow e_{aq}^-$	2.51×10^7	$e_{aq}^- + H_3O^+ \rightarrow H^\bullet$	2.11×10^{10}
$H^\bullet + O_2 \rightarrow HO_2^\bullet$	2.1×10^{10}	$e_{aq}^- + O_2^{\bullet-} \rightarrow H_2O_2 + 2OH^-$	1.3×10^{10}
$H^\bullet + HO_2^\bullet \rightarrow H_2O_2$	1.0×10^{10}	$e_{aq}^- + HO_2^- \rightarrow O^{\bullet-} + OH^-$	3.51×10^9
$H^\bullet + O_2^{\bullet-} \rightarrow HO_2^-$	1.0×10^{10}	$e_{aq}^- + O_2 \rightarrow O_2^{\bullet-}$	1.74×10^{10}
$\bullet OH + \bullet OH \rightarrow H_2O_2$	5.5×10^9	$e_{aq}^- + HO_2^\bullet \rightarrow HO_2^-$	1.28×10^{10}
$\bullet OH + H_2O_2 \rightarrow HO_2^\bullet$	2.87×10^7	$H_3O^+ + O_2^{\bullet-} \rightarrow HO_2^\bullet$	4.78×10^{10}
$\bullet OH + H_2 \rightarrow H^\bullet$	3.28×10^7	$H_3O^+ + OH^- \rightarrow$ No product	1.12×10^{11}
$\bullet OH + e_{aq}^- \rightarrow OH^-$	2.95×10^{10}	$H_3O^+ + HO_2^- \rightarrow H_2O_2$	5.0×10^{10}
$\bullet OH + OH^- \rightarrow O^{\bullet-}$	6.3×10^9	$HO_2^\bullet + O_2^{\bullet-} \rightarrow O_2 + HO_2^-$	9.7×10^7
$\bullet OH + HO_2^\bullet \rightarrow O_2$	7.9×10^9	$HO_2^\bullet + HO_2^\bullet \rightarrow O_2 + H_2O_2$	8.3×10^5
$\bullet OH + O_2^{\bullet-} \rightarrow OH^- + O_2$	1.07×10^{10}	$HO_2^\bullet + O(^3P) \rightarrow O_2 + \bullet OH$	2.02×10^{10}
$\bullet OH + HO_2^- \rightarrow OH^- + HO_2^\bullet$	8.32×10^9	$O(^3P) + O(^3P) \rightarrow O_2$	2.2×10^{10}
$\bullet OH + O^{\bullet-} \rightarrow HO_2^-$	1.0×10^9	$O^{\bullet-} + H_2O \rightarrow \bullet OH + OH^-$	$1.36 \times 10^6\ (s^{-1})$
$\bullet OH + O(^3P) \rightarrow HO_2^\bullet$	2.02×10^{10}	$HO_2^- + H_2O \rightarrow H_2O_2 + OH^-$	$1.36 \times 10^6\ (s^{-1})$

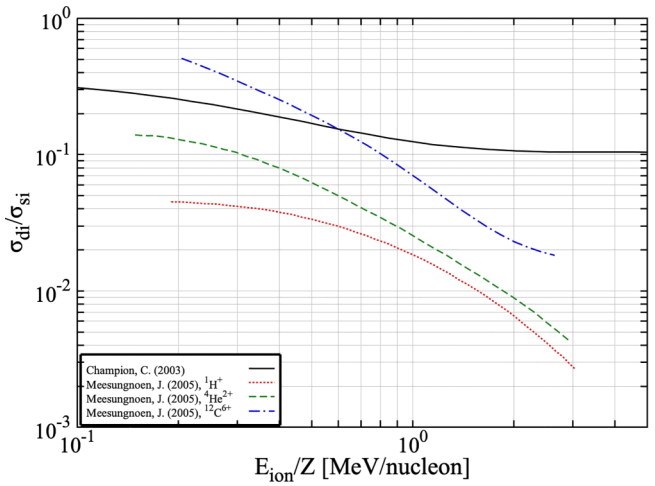

FIG. 1. The ratio of double-to-single ionization cross sections σ_{di}/σ_{si} for $^{1}H^{+}$ (dotted red line), $^{4}He^{2+}$ (dashed green line), and $^{12}C^{6+}$ (dashed-dotted blue line) ion beams reported by Meesungnoen and Jay-Gerin.[11] The values of σ_{di}/σ_{si} reported by Champion[25] for a variety of ions at intermediate velocities and gaseous water are also shown for the sake of comparison (solid black line).

$^{4}He^{2+}$ ion beam agree with the experimental results obtained by Pastina and LaVerne,[34] Burns and Sims,[33] and Anderson and Hart.[31] In the case of the $^{12}C^{6+}$ ion beam, when considering multiple ionization processes (solid line), the G-value of H_2O_2 rises monotonically up to 200 eV/nm and then decreases. Above 200 eV/nm, the simulated G-values for the $^{12}C^{6+}$ ion beam are significantly smaller than the experimental results reported by Pastina and LaVerne.[34] To reproduce experimental results using the simulation around Bragg peak energies, we adopt the differential values of the number of water radiolysis species N over the ion trajectory at the energy of incident ions E_0 to the G-values and plotted them as a function of the track average LET, which is defined as $\overline{LET} = 1/E_0 \int_0^{E_0} (dE/dx)dE$.[34] The G-value of H_2O_2 for full stop condition of the $^{12}C^{6+}$ ion beam is also represented in Fig. 2 (dashed-dotted magenta line). Experimental results are in this way well reproduced by the simulation.

The cross sections of double ionization increase with increasing LET (i.e., decreasing energy of incoming ion) (Fig. 1), and oxygen atoms are formed in their 3P ground-state $O(^3P)$ by multiple ionization in the high-LET region. Typically, H_2O_2 is produced by the reaction between •OHs (i.e., $\bullet OH + \bullet OH \rightarrow H_2O_2$). However, in the high-LET region, •OH reacts not only with other •OH but also with $O(^3P)$ ($\bullet OH + O(^3P) \rightarrow HO_2^{\bullet}$), and the yields of H_2O_2 drop in the high-LET region, especially significant above 200 eV/nm.

Figure 3 shows the LET dependence of the G-value of $HO_2^{\bullet} + O_2^{\bullet -}$ at 1 μs after irradiation. Solid lines represent the trends obtained by Genat4-DNA simulation with the multiple ionization processes. Experimental results are plotted by open symbols.[38,39] The dashed and dashed-dotted-dotted lines represent previous simulation results with the multiple ionization

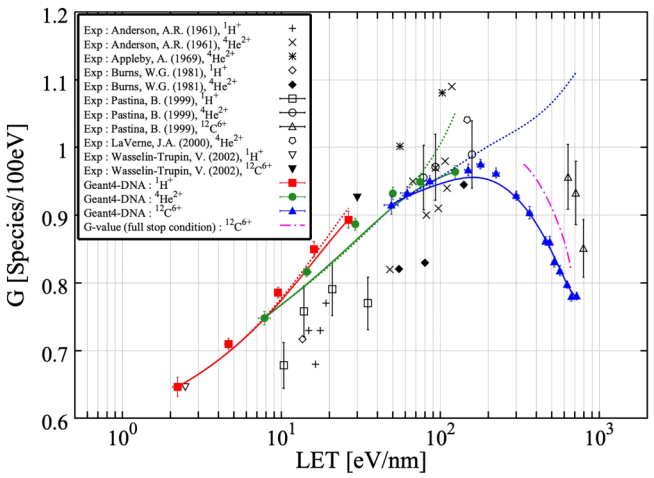

FIG. 2. LET dependence of G-values of H_2O_2 by $^{1}H^{+}$ (red square), $^{4}He^{2+}$ (green circle), and $^{12}C^{6+}$ (blue triangle) ion beams with multiple ionization processes (solid line) and without multiple ionization processes (dotted line) at 1 μs after irradiation. Solid and dotted lines represent the trends obtained by Genat4-DNA simulation with and without the multiple ionization processes, respectively. The G-value of H_2O_2 by full stop condition of $^{12}C^{6+}$ ion beams with multiple ionization processes is shown with the dashed-dotted magenta line. Experimental data presented by Anderson and Hart,[31] Appleby and Schwarz,[32] Burns and Sims,[33] Pastina and LaVerne,[34] LaVerne *et al.*,[35] and Wasselin-Trupin *et al.*[36] are used for comparison with simulated LET dependence of G-values.

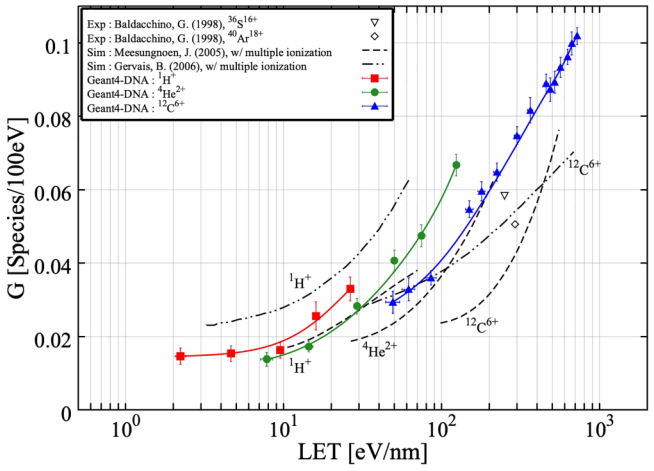

FIG. 3. LET dependence of G-values of $HO_2^{\bullet} + O_2^{\bullet -}$ by $^{1}H^{+}$ (red square), $^{4}He^{2+}$ (green circle), and $^{12}C^{6+}$ (blue triangle) ion beams with multiple ionization processes (solid line) at 1 μs after irradiation. Solid lines represent the trends obtained by Genat4-DNA simulation with the multiple ionization processes. The dashed and dashed-dotted-dotted black lines represent present simulation results with the multiple ionization processes reported by Meesungnoen and Jay-Gerin[11] and Gervais *et al.*,[12] respectively. Sets of experimental data presented by Baldacchino *et al.*[38,39] were used for comparison with simulated LET dependence of G-values.

processes reported by Meesungnoen and Jay-Gerin[11] and Gervais *et al.*,[12] respectively. The G-values of $HO_2^{\bullet} + O_2^{\bullet -}$ for $^1H^+$ ion beams evaluated in the present study are between the previous simulations. Also, the present G-values of $HO_2^{\bullet} + O_2^{\bullet -}$ for $^4He^{2+}$ and $^{12}C^{6+}$ ion beams are higher than the previous results at the same LETs. At the same LET, the G-value of $HO_2^{\bullet} + O_2^{\bullet -}$ for lighter ions is higher than those of heavier ones. This is because the velocity of lighter ions is slower than that of heavier ones, thereby higher local energy deposition at the close location from the ion path can be expected by lighter ions.[40,41] Our simulation results for $^{12}C^{6+}$ ion beams are higher than the experimental results under $^{36}S^{16+}$ and $^{40}Ar^{18+}$ ion beams. This finding would support the reliability of our simulation. The simulated G-values increase monotonically with increasing LET, rising more rapidly

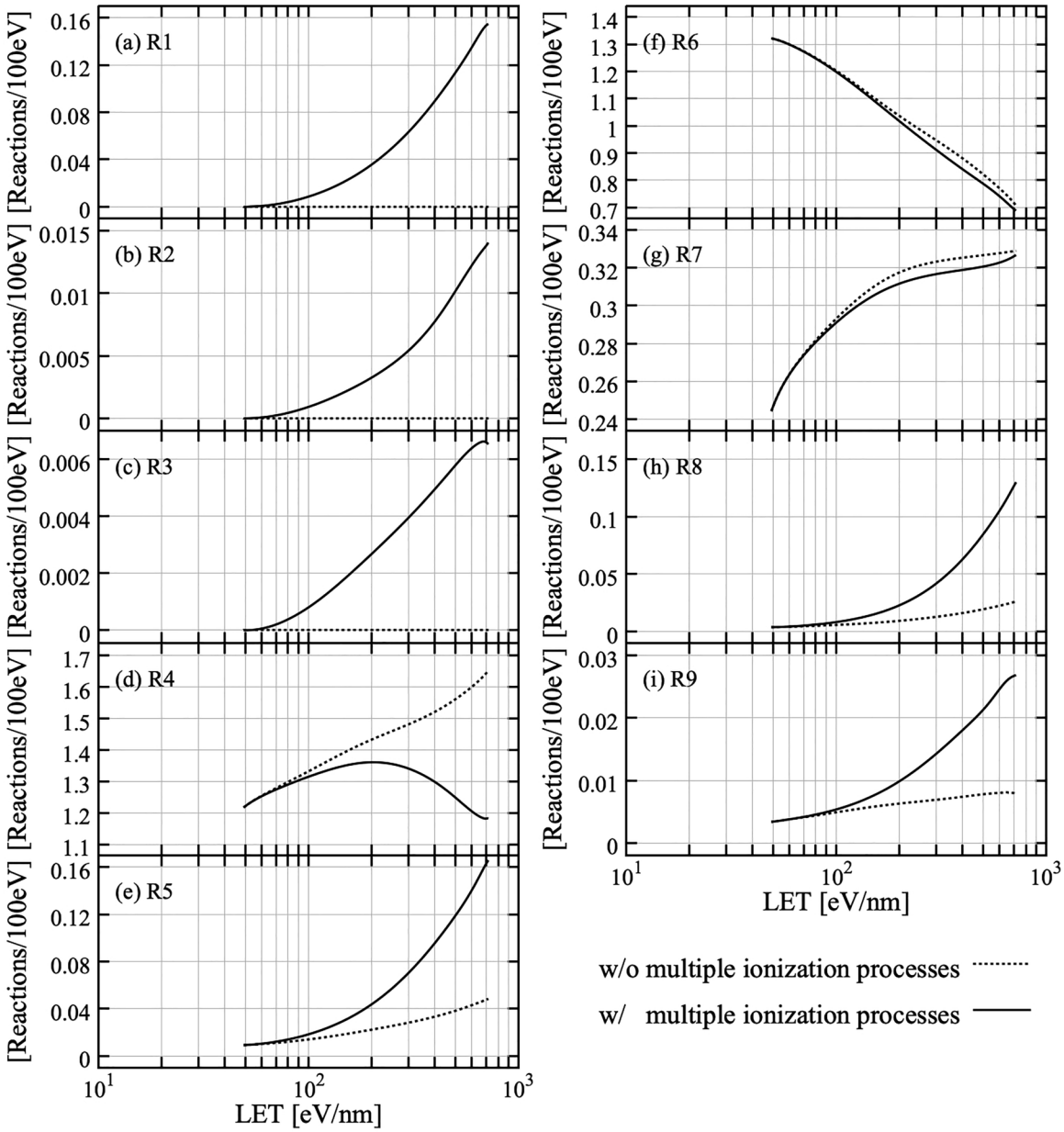

FIG. 4. LET dependence of each chemical reaction number by $^{12}C^{6+}$ ion beams without multiple ionization processes (dotted line) and with multiple ionization processes (solid line) at 1 μs after irradiation.

above 200 eV/nm, where the G-value of H_2O_2 begins dropping. In fact, •OH reacts not only with $O(^3P)$ but also with $HO_2^{\bullet}$ ($\bullet OH + HO_2^{\bullet} \rightarrow O_2$). Therefore, above 200 eV/nm, the consumption of •OH by the reaction with $O(^3P)$ (R1) and $HO_2^{\bullet}$ (R5) is competitive processes with the generation of H_2O_2 by the reaction between •OHs (R4). As a result, the G-value of H_2O_2 reduces above 200 eV/nm. This result is reasonable because the biological effectiveness increases due to the radiation-induced oxygen produced along the ion trajectory in the high-LET region.

Figure 4 shows the LET dependence of several chemical reactions with and without the multiple ionization processes at 1 μs after irradiation. H_2O_2 is formed along the ion path by reaction (R4) (see the reaction list below). At LET above 200 eV/nm, the ground-state $O(^3P)$ atoms are inert to water molecules. However, $O(^3P)$ atoms efficiently react with •OH (R1) in the track core of heavy ions, at which relatively high concentrations of water radiolysis products can be expected. O_2 is generated by the reaction of $HO_2^{\bullet}$ with •OH (R5),

$$\bullet OH + \bullet OH \rightarrow H_2O_2 \quad 5.5 \times 10^9\ (dm^3\ mol^{-1}\ s^{-1}), \tag{R4}$$

$$HO_2^{\bullet} + \bullet OH \rightarrow O_2 + H_2O \quad 7.9 \times 10^9\ (dm^3\ mol^{-1}\ s^{-1}), \tag{R5}$$

$$\bullet OH + e_{aq}^- \rightarrow OH^- \quad 2.95 \times 10^{10}\ (dm^3\ mol^{-1}\ s^{-1}), \tag{R6}$$

$$H_2O_2 + e_{aq}^- \rightarrow OH^- + \bullet OH \quad 1.1 \times 10^{10}\ (dm^3\ mol^{-1}\ s^{-1}), \tag{R7}$$

$$H^{\bullet} + O_2 \rightarrow HO_2^{\bullet} \quad 2.1 \times 10^{10}\ (dm^3\ mol^{-1}\ s^{-1}), \tag{R8}$$

$$e_{aq}^- + O_2 \rightarrow O_2^{\bullet -} \quad 1.74 \times 10^{10}\ (dm^3\ mol^{-1}\ s^{-1}). \tag{R9}$$

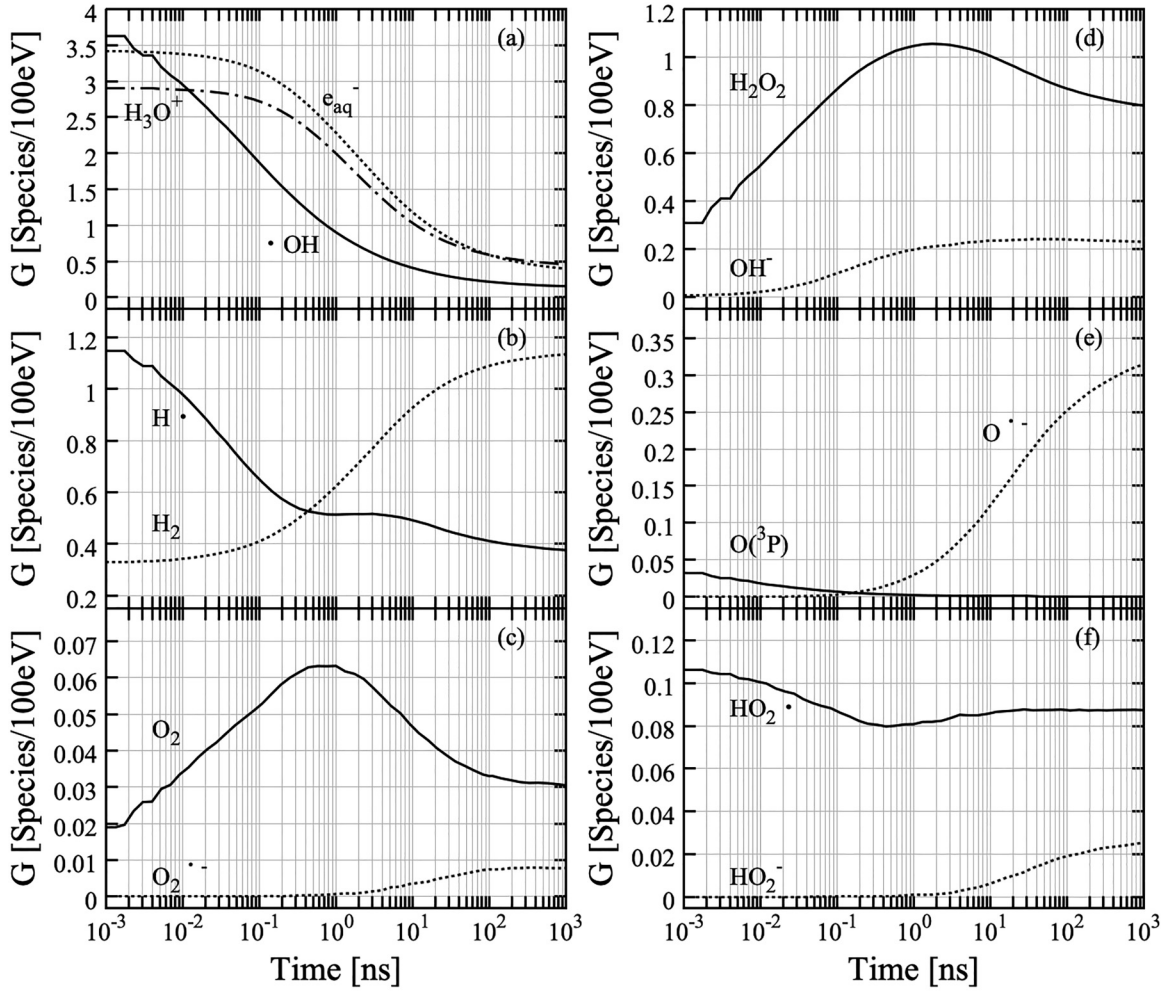

FIG. 5. The time dependence of G-values of water radiolysis species for 12 MeV $^{12}C^{6+}$ ion beams with multiple ionization processes in the time 1 ps to 1 μs.

By competing with reaction (R4), reactions (R1) and (R5) cause a decrease in the number of H_2O_2 generated and an increase in the number of $HO_2^{\bullet} + O_2^{\bullet-}$ formed in the high-LET region. It was also confirmed that the reactions of e_{aq}^- with •OH (R6) and H_2O_2 (R7) contribute to the reduction of H_2O_2. The contribution of reaction (R6) decreases with increasing LET because other radical–radical reactions (e.g., $\bullet OH + \bullet OH \rightarrow H_2O_2$ and $H^{\bullet} + {}^{\bullet}OH \rightarrow H_2O$) increase. With multiple ionization, the contribution of reaction (R6) is lower than that without multiple ionization. This finding implies that •OH reacts with $O(^3P)$ ($\bullet OH + O(^3P) \rightarrow HO_2^{\bullet}$). Also, as LET increases, the contribution of reaction (R7) increases, resulting in a decrease in H_2O_2. Among the reactions considered in this study, reaction (R7) has the largest reaction rate constant $1.1 \times 10^{10}\ dm^3\ mol^{-1}\ s^{-1}$ among the direct reactions with H_2O_2. The contribution of reaction (R7) with multiple ionization is slightly lower than that without multiple ionization. However, the contribution of reaction (R7) is significant because the G-value of H_2O_2 starts decreasing above 200 eV/nm. Atomic oxygen $O(^3P)$ with the ground state is produced by multiple ionization. It is clear that the multiple ionization processes play an important role in the formation of $HO_2^{\bullet}$ and $O_2^{\bullet-}$ through the generation of atomic oxygen with the ground-state $O(^3P)$. Therefore, the reaction probabilities of reactions (R1) and (R5) increase, resulting in the facilitation of the generation of $HO_2^{\bullet}$ and $O_2^{\bullet-}$. Furthermore, under the multiple ionization processes, O_2 is consumed by secondary reactions, for instance, by reactions (R8) and (R9).

Figure 5 shows the time dependence of G-values of water radiolysis species for a 12 MeV $^{12}C^{6+}$ ion beam with the multiple ionization processes. The G-values of e_{aq}^-, H_3O^+, and •OH decrease monotonically with time. That of $H^{\bullet}$ also decreases with time. With the reduction of $H^{\bullet}$, the G-value of H_2 increases. This trend would be related to the $H^{\bullet} + H^{\bullet} \rightarrow H_2$ reaction. The formation of O_2 can be seen by the intra-track reaction in the high-LET region. 1 ns after irradiation, the G-value of O_2 decreases with time due to the reaction with $H^{\bullet}$ ($H^{\bullet} + O_2 \rightarrow HO_2^{\bullet}$) and e_{aq}^- ($e_{aq}^- + O_2 \rightarrow O_2^{\bullet-}$). These reactions contribute the formation of $HO_2^{\bullet}$ and $O_2^{\bullet-}$. H_2O_2 increases with time up to several ns and then slowly drops. The G-value of OH^- increases gradually and becomes almost constant above 1 ns. The G-value of $O(^3P)$ is smaller, but it is certainly formed at the early chemical stage. The $O(^3P)$ produced decreases with time. This trend would be related to the formation of O_2. Finally, we confirm the formation of $O^{\bullet-}$ and HO_2^- in the chemical stage.

Whereas discrepancies are observed between simulations without multiple ionization and experiments, the G-value of H_2O_2 agrees with experimental results by adding the multiple ionization processes. We have also succeeded in reproducing experimental results of the G-value of $HO_2^{\bullet} + O_2^{\bullet-}$ by implementing the multiple ionization processes. These results support the importance of multiple ionization in the radiolysis of water under high-LET irradiation.

CONCLUSION

The role of multiple ionization in water influencing the G-values of the radiolytic free radical and molecular species, including O_2, was investigated using a Monte Carlo code based on Geant4-DNA. Considering the multiple ionization processes of water molecules, the G-values of H_2O_2 and $HO_2^{\bullet} + O_2^{\bullet-}$ were calculated as a function of LET. The simulated G-value of H_2O_2 increased monotonically with increasing LET up to 200 eV/nm, then dropped. This trend was in agreement with experimental results. Additionally, we succeeded in reproducing the G-value of $HO_2^{\bullet} + O_2^{\bullet-}$. $O(^3P)$ generated by multiple ionization effects, which leads to the reaction with •OH ($\bullet OH + O(^3P) \rightarrow HO_2^{\bullet}$). A reduction of H_2O_2 yield in the high-LET region above 200 eV/nm can be explained by the consumption of the •OH radicals by other radical–radical reactions due to multiple ionization. Furthermore, under the multiple ionization processes, O_2 is consumed by secondary reactions. The consumption of O_2 and the role of multiple ionization are crucial to explain the FLASH effect.

ACKNOWLEDGMENTS

This work was supported by JSPS KAKENHI under Grant No. JP19H03594.

DATA AVAILABILITY

The data that support the findings of this study are available from the corresponding authors upon reasonable request.

REFERENCES

[1]E. Scifoni, W. Tinganelli, W. K. Weyrather, M. Durante, A. Maier, and M. Krämer, Phys. Med. Biol. **58**, 3871 (2013).
[2]T. Alper, Radiat. Res. **5**, 573 (1956).
[3]Y. Furusawa, K. Fukutsu, M. Aoki, H. Itsukaichi, K. Eguchi-Kasai, H. Ohara, F. Yatagai, T. Kanai, and K. Ando, Radiat. Res. **154**, 485–496 (2000).
[4]K. Ando, S. Koike, C. Ohira, Y. J. Chen, K. Nojima, S. Ando, T. Ohbuchi, N. Kobayashi, W. Shimizu, and M. Urano, Int. J. Radiat. Biol. **75**, 505 (1999).
[5]R. Hirayama, A. Uzawa, N. Takase, Y. Matsumoto, M. Noguchi, K. Koda, M. Ozaki, K. Yamashita, H. Li, Y. Kase, N. Matsufuji, S. Koike, S.-i. Masunaga, K. Ando, R. Okayasu, and Y. Furusawa, Mutat. Res., Genet. Toxicol. Environ. Mutagen. **756**, 146 (2013).
[6]T. Kusumoto, H. Kitamura, S. Hojo, T. Konishi, and S. Kodaira, RSC Adv. **10**, 38709 (2020).
[7]Y. Lai, X. Jia, and Y. Chi, Phys. Med. Biol. **66**, 025004 (2021).
[8]G. Pratx and D. S. Kapp, Phys. Med. Biol. **64**, 185005 (2019).
[9]G. Adrian, E. Konradsson, M. Lempart, S. Bäck, C. Ceberg, and K. Petersson, Br. J. Radiol. **93**, 20190702 (2020).
[10]J. Meesungnoen, A. Filali-Mouhim, N. S. N. Ayudhya, S. Mankhetkorn, and J.-P. Jay-Gerin, Chem. Phys. Lett. **377**, 419 (2003).
[11]J. Meesungnoen and J.-P. Jay-Gerin, J. Phys. Chem. A **109**, 6406 (2005).
[12]B. Gervais, M. Beuve, G. H. Olivera, and M. E. Galassi, Radiat. Phys. Chem. **75**, 493 (2006).
[13]K. Baba, T. Kusumoto, S. Okada, R. Ogawara, S. Kodaira, Q. Raffy, R. Barillon, N. Ludwig, C. Galindo, P. Peaupardin, and M. Ishikawa, Sci. Rep. **11**, 1 (2021).
[14]S. Agostinelli, J. Allison, K. Amako, J. Apostolakis, H. Araujo, P. Arce, M. Asai, D. Axen, S. Banerjee, G. Barrand, F. Behner, L. Bellagamba, J. Boudreau, L. Broglia, A. Brunengo, H. Burkhardt, S. Chauvie, J. Chuma, R. Chytracek, G. Cooperman, G. Cosmo, P. Degtyarenko, A. Dell'Acqua, G. Depaola, D. Dietrich, R. Enami, A. Feliciello, C. Ferguson, H. Fesefeldt, G. Folger, F. Foppiano, A. Forti, S. Garelli, S. Giani, R. Giannitrapani, D. Gibin, J. J. Gómez Cadenas, I. González, G. Gracia Abril, G. Greeniaus, W. Greiner, V. Grichine, A. Grossheim, S. Guatelli, P. Gumplinger, R. Hamatsu, K. Hashimoto, H. Hasui, A. Heikkinen, A. Howard, V. Ivanchenko, A. Johnson, F. W. Jones, J. Kallenbach, N. Kanaya, M. Kawabata, Y. Kawabata, M. Kawaguti, S. Kelner, P. Kent, A. Kimura, T. Kodama, R. Kokoulin, M. Kossov, H. Kurashige, E. Lamanna, T. Lampén, V. Lara, V. Lefebure, F. Lei, M. Liendl, W. Lockman, F. Longo, S. Magni, M. Maire, E. Medernach, K. Minamimoto,

P. Mora de Freitas, Y. Morita, K. Murakami, M. Nagamatu, R. Nartallo, P. Nieminen, T. Nishimura, K. Ohtsubo, M. Okamura, S. O'Neale, Y. Oohata, K. Paech, J. Perl, A. Pfeiffer, M. G. Pia, F. Ranjard, A. Rybin, S. Sadilov, E. Di Salvo, G. Santin, T. Sasaki, N. Savvas, Y. Sawada, S. Scherer, S. Sei, V. Sirotenko, D. Smith, N. Starkov, H. Stoecker, J. Sulkimo, M. Takahata, S. Tanaka, E. Tcherniaev, E. Safai Tehrani, M. Tropeano, P. Truscott, H. Uno, L. Urban, P. Urban, M. Verderi, A. Walkden, W. Wander, H. Weber, J. P. Wellisch, T. Wenaus, D. C. Williams, D. Wright, T. Yamada, H. Yoshida, and D. Zschiesche, Nucl. Instrum. Methods Phys. Res., Sect. A **506**, 250 (2003).

[15]J. Allison, K. Amako, J. Apostolakis, H. Araujo, P. Arce Dubois, M. Asai, G. Barrand, R. Capra, S. Chauvie, R. Chytracek, G. A. P. Cirrone, G. Cooperman, G. Cosmo, G. Cuttone, G. G. Daquino, M. Donszelmann, M. Dressel, G. Folger, F. Foppiano, J. Generowicz, V. Grichine, S. Guatelli, P. Gumplinger, A. Heikkinen, I. Hrivnacova, A. Howard, S. Incerti, V. Ivanchenko, T. Johnson, F. Jones, T. Koi, R. Kokoulin, M. Kossov, H. Kurashige, V. Lara, S. Larsson, F. Lei, O. Link, F. Longo, M. Maire, A. Mantero, B. Mascialino, I. McLaren, P. Mendez Lorenzo, K. Minamimoto, K. Murakami, P. Nieminen, L. Pandola, S. Parlati, L. Peralta, J. Perl, A. Pfeiffer, M. G. Pia, A. Ribon, P. Rodrigues, G. Russo, S. Sadilov, G. Santin, T. Sasaki, D. Smith, N. Starkov, S. Tanaka, E. Tcherniaev, B. Tome, A. Trindade, P. Truscott, L. Urban, M. Verderi, A. Walkden, J. P. Wellisch, D. C. Williams, D. Wright, and H. Yoshida, IEEE Trans. Nucl. Sci. **53**, 270 (2006).

[16]J. Allison, K. Amako, J. Apostolakis, P. Arce, M. Asai, T. Aso, E. Bagli, A. Bagulya, S. Banerjee, G. Barrand, B. R. Beck, A. G. Bogdanov, D. Brandt, J. M. C. Brown, H. Burkhardt, P. Canal, D. Cano-Ott, S. Chauvie, K. Cho, G. A. P. Cirrone, G. Cooperman, M. A. Cortés-Giraldo, G. Cosmo, G. Cuttone, G. Depaola, L. Desorgher, X. Dong, A. Dotti, V. D. Elvira, G. Folger, Z. Francis, A. Galoyan, L. Garnier, M. Gayer, K. L. Genser, V. M. Grichine, S. Guatelli, P. Guèye, P. Gumplinger, A. S. Howard, I. Hřivnáčová, S. Hwang, S. Incerti, A. Ivanchenko, V. N. Ivanchenko, F. W. Jones, S. Y. Jun, P. Kaitaniemi, N. Karakatsanis, M. Karamitros, M. Kelsey, A. Kimura, T. Koi, H. Kurashige, A. Lechner, S. B. Lee, F. Longo, M. Maire, D. Mancusi, A. Mantero, E. Mendoza, B. Morgan, K. Murakami, T. Nikitina, L. Pandola, P. Paprocki, J. Perl, I. Petrović, M. G. Pia, W. Pokorski, J. M. Quesada, M. Raine, M. A. Reis, A. Ribon, A. Ristić Fira, F. Romano, G. Russo, G. Santin, T. Sasaki, D. Sawkey, J. I. Shin, I. I. Strakovsky, A. Taborda, S. Tanaka, B. Tomé, T. Toshito, H. N. Tran, P. R. Truscott, L. Urban, V. Uzhinsky, J. M. Verbeke, M. Verderi, B. L. Wendt, H. Wenzel, D. H. Wright, D. M. Wright, T. Yamashita, J. Yarba, and H. Yoshida, Nucl. Instrum. Methods Phys. Res., Sect. A **835**, 186 (2016).

[17]S. Incerti, I. Kyriakou, M. A. Bernal, M. C. Bordage, Z. Francis, S. Guatelli, V. Ivanchenko, M. Karamitros, N. Lampe, S. B. Lee, S. Meylan, C. H. Min, W. G. Shin, P. Nieminen, D. Sakata, N. Tang, C. Villagrasa, H. N. Tran, and J. M. C. Brown, Med. Phys. **45**, e722 (2018).

[18]S. Incerti, G. Baldacchino, M. Bernal, R. Capra, C. Champion, Z. Francis, P. GuÊye, A. Mantero, B. Mascialino, P. Moretto, P. Nieminen, C. Villagrasa, and C. Zacharatou, Int. J. Model. Simul. Sci. Comput. **1**, 157 (2010).

[19]S. Incerti, A. Ivanchenko, M. Karamitros, A. Mantero, P. Moretto, H. N. Tran, B. Mascialino, C. Champion, V. N. Ivanchenko, M. A. Bernal, Z. Francis, C. Villagrasa, G. Baldacchino, P. Guèye, R. Capra, P. Nieminen, and C. Zacharatou, Med. Phys. **37**, 4692 (2010).

[20]M. A. Bernal, M. C. Bordage, J. M. C. Brown, M. Davídková, E. Delage, Z. El Bitar, S. A. Enger, Z. Francis, S. Guatelli, V. N. Ivanchenko, M. Karamitros, I. Kyriakou, L. Maigne, S. Meylan, K. Murakami, S. Okada, H. Payno, Y. Perrot, I. Petrovic, Q. T. Pham, A. Ristic-Fira, T. Sasaki, V. Štěpán, H. N. Tran, C. Villagrasa, and S. Incerti, Phys. Med. **31**, 861 (2015).

[21]M. Karamitros, A. Mantero, S. Incerti, W. Friedland, G. Baldacchino, P. Barberet, M. Bernal, R. Capra, C. Champion, Z. El Bitar, Z. Francis, P. Guèye, A. Ivanchenko, V. Ivanchenko, H. Kurashige, B. Mascialino, P. Moretto, P. Nieminen, G. Santin, H. Seznec, H. N. Tran, C. Villagrasa, and C. Zacharatou, Prog. Nucl. Sci. Technol. **2**, 503 (2011).

[22]M. Karamitros, S. Luan, M. A. Bernal, J. Allison, G. Baldacchino, M. Davidkova, Z. Francis, W. Friedland, V. Ivantchenko, A. Ivantchenko, A. Mantero, P. Nieminem, G. Santin, H. N. Tran, V. Stepan, and S. Incerti, J. Comput. Phys. **274**, 841 (2014).

[23]M. E. Rudd, Radiat. Prot. Dosim. **31**, 17 (1990).

[24]V. Cobut, Y. Frongillo, J. P. Patau, T. Goulet, M.-J. Fraser, and J.-P. Jay-Gerin, Radiat. Phys. Chem. **51**, 229 (1998).

[25]C. Champion, Nucl. Instrum. Methods Phys. Res., Sect. B **205**, 671 (2003).

[26]J. Meesungnoen and J.-P. Jay-Gerin, Radiat. Res. **164**, 688 (2005).

[27]J. Meesungnoen and J.-P. Jay-Gerin, Radiat. Res. **171**, 379 (2009).

[28]Y. Hatano, Y. Katsumura, and A. Mozumder, *Charged Particle and Photon Interactions with Matter: Recent Advances, Applications, and Interfaces* (CRC Press, 2011).

[29]I. Plante, Radiat. Environ. Biophys. **50**, 389 (2011).

[30]W. G. Shin, J. Ramos-Mendez, B. Faddegon, H. N. Tran, C. Villagrasa, Y. Perrot, S. Okada, M. Karamitros, D. Emfietzoglou, I. Kyriakou, M. C. Bordage, D. Sakata, S. Guatelli, H. J. Choi, C. H. Min, S. B. Lee, and S. Incerti, J. Appl. Phys. **126**, 114301 (2019).

[31]A. R. Anderson and E. J. Hart, Radiat. Res. **14**, 689 (1961).

[32]A. Appleby and H. A. Schwarz, J. Phys. Chem. **73**, 1937 (1969).

[33]W. G. Burns and H. E. Sims, J. Chem. Soc., Faraday Trans. 1 **77**, 2803 (1981).

[34]B. Pastina and J. A. LaVerne, J. Phys. Chem. A **103**, 1592 (1999).

[35]J. A. LaVerne, in *Proceedings of 11th International Congress of Radiation Research, Dublin, Ireland, 18–23 July 1999*, edited by M. Moriarty, C. Mothersill, C. Seymour, M. Edington, J. F. Ward, and R. J. M. Fry (Allen Press, Lawrence, KS, 2000), Vol. 2.

[36]V. Wasselin-Trupin, G. Baldacchino, S. Bouffard, and B. Hickel, Radiat. Phys. Chem. **65**, 53 (2002).

[37]M. Taguchi and T. Kojima, Nucl. Sci. Tech. **18**, 35 (2007).

[38]G. Baldacchino, D. Le Parc, B. Hickel, M. Gardes-Albert, Z. Abedinzadeh, D. Jore, S. Deycard, S. Bouffard, V. Mouton, and E. Balanzat, Radiat. Res. **149**, 128 (1998).

[39]G. Baldacchino, S. Bouffard, E. Balanzat, M. Gardès-Albert, Z. Abedinzadeh, D. Jore, S. Deycard, and B. Hickel, Nucl. Instrum. Methods Phys. Res., Sect. B **146**, 528 (1998).

[40]M. P. R. Waligórski, R. N. Hamm, and R. Katz, Int. J. Radiat. Appl. Instrum. **11**, 309 (1986).

[41]T. Kusumoto, Y. Mori, M. Kanasaki, R. Ikenaga, K. Oda, S. Kodaira, H. Kitamura, R. Barillon, and T. Yamauchi, Radiat. Meas. **87**, 35 (2016).